

Quasinormal modes of Reissner-Nordström-anti-de Sitter black holes: scalar, electromagnetic and gravitational perturbations

E. Berti and K.D. Kokkotas

Department of Physics, Aristotle University of Thessaloniki, Thessaloniki 54124, Greece

(Dated: October 22, 2018)

We study scalar, electromagnetic and gravitational perturbations of a Reissner-Nordström-anti-de Sitter (RN-AdS) spacetime, and compute its quasinormal modes (QNM's). We confirm and extend results previously found for Schwarzschild-anti-de Sitter (S-AdS) black holes. For “large” black holes, whose horizon is much larger than the AdS radius, different classes of perturbations are almost exactly *isospectral*; this isospectrality is broken when the black hole's horizon radius is comparable to the AdS radius. We provide very accurate fitting formulas for the QNM's, which are valid for large black holes having charge $Q < Q_{ext}/3$ (Q_{ext} being the extremal value of the charge).

Electromagnetic and axial perturbations of large black holes are characterized by the existence of pure-imaginary (purely damped) modes. The damping of these modes tends to infinity as the black hole charge approaches the extremal value; if the corresponding mode amplitude does not tend to zero in the same limit, this implies that *extremally charged RN-AdS black holes are marginally unstable*. This result is relevant in view of the AdS/CFT conjecture, since, according to it, the AdS QNM's give the timescales for approach to equilibrium in the corresponding conformal field theory.

1. INTRODUCTION

Quasinormal modes (QNM's) are well known to play an important role in black hole physics. They determine the late-time evolution of fields in the black hole exterior, and numerical simulations of stellar collapse and black hole collisions have shown that in the final stage of such processes (“ringdown”) the quasinormal modes eventually dominate the black hole response to any kind of perturbation. For these reasons, QNM's of black holes in asymptotically flat spacetime have been extensively studied for more than thirty years (for comprehensive reviews see [1, 2]).

Perturbations of non-asymptotically flat spacetimes have also been studied for years in a cosmological context. For example, perturbations of Schwarzschild-de Sitter spacetimes were considered in [3], and the corresponding QNM's were computed in [4]. An analogous study for Reissner-Nordström-de Sitter perturbations was performed in [5].

In the last few years, the anti-de Sitter (AdS) conformal field theory (CFT) conjecture has led to an intensive investigation of black hole QNM's in asymptotically AdS spacetimes. According to the AdS/CFT correspondence [6], a large static black hole in asymptotically AdS spacetime corresponds to an (approximately) thermal state in the CFT. So the time scale for the decay of the black hole perturbation, which is given by the imaginary part of its QNM's, corresponds to the timescale to reach thermal equilibrium in the strongly coupled CFT [7]. The computation of these time scales in the CFT is a difficult task. Therefore, black hole perturbation theory has turned out to be, quite unexpectedly, a useful tool to compute CFT thermalization time scales.

Quasinormal modes in AdS spacetime were first computed for a conformally invariant scalar field, whose asymptotic behaviour is similar to flat spacetime, in [8]. Subsequently, motivated by the AdS-CFT correspondence, Horowitz and Hubeny made a systematic computation of QNM's for scalar perturbations of Schwarzschild-AdS (S-AdS) spacetimes [9]. Their work was extended to gravitational and electromagnetic perturbations of S-AdS black holes in [10]. A reconsideration of the correct boundary conditions for the QNM problem was presented by Moss and Norman [11], who considered gravitational perturbations of both Schwarzschild-de Sitter and S-AdS spacetimes. Finally, the study of scalar perturbations was extended to the case of Reissner-Nordström-AdS (RN-AdS) black holes in [12].

Frequency-domain studies of de Sitter and anti-de Sitter black hole spacetimes have lately been complemented by time evolutions. In [13] and [14], the authors used a time evolution approach to study tails in Schwarzschild-de Sitter backgrounds from a cosmological perspective. Motivated by the AdS/CFT correspondence, analogous time evolutions have recently been performed for RN-AdS backgrounds in [15].

Numerical methods used so far to compute QNM's in AdS backgrounds tend to break down, in the S-AdS case, as the black hole horizon becomes much smaller than the AdS radius [9]. Therefore, special attention has been devoted to the small-black hole limit, using both a frequency domain [16] and a time domain approach [17].

Our aim in this paper is to present a comprehensive study of scalar, electromagnetic and gravitational perturbations of RN-AdS black holes in the frequency domain. We verify (or sometimes disprove) and extend many results obtained in the aforementioned papers. We also compute for the first time electromagnetic and gravitational QNM's for RN-AdS black holes, building on work done previously in the cosmological context for Reissner-Nordström-de Sitter

spacetimes [5].

The plan of the paper is as follows. In section 2 we introduce our notation for the background metric, display explicitly the wave equations describing scalar, electromagnetic and gravitational perturbations, and briefly present our numerical methods and conventions. Details on the numerical methods are deferred to the Appendix. In section 3 we first summarize and extend some well-known results for perturbations of S-AdS black holes, considering all three cases (scalar, electromagnetic and gravitational perturbations); then we use the uncharged case as a starting point to discuss perturbations of RN-AdS black holes, and present most of our new numerical results. The conclusions and a discussion follow.

2. PERTURBATION EQUATIONS IN A RN-ADS BACKGROUND

2.1. Background

We are interested in scalar, electromagnetic and gravitational perturbations of a Reissner-Nordström anti-de Sitter metric,

$$ds^2 = f(r)dt^2 - \frac{dr^2}{f(r)} - r^2(d\theta^2 + \sin^2\theta d\phi^2), \quad (1)$$

where $f(r) = \Delta/r^2$ and

$$\Delta = r^2 - 2Mr + Q^2 + \frac{r^4}{R^2}. \quad (2)$$

In the previous formulas M is the black hole mass, Q the black hole charge, and R is the AdS radius. The black hole mass is related to its charge Q and horizon radius r_+ by the relation

$$M = \frac{1}{2} \left(r_+ + \frac{r_+^3}{R^2} + \frac{Q^2}{r_+} \right), \quad (3)$$

while the black hole's Hawking temperature is given by

$$T = \frac{1 - Q^2/r_+^2 + 3r_+^2/R^2}{4\pi r_+}. \quad (4)$$

It will be useful in the following to introduce a tortoise coordinate r_* , defined in the usual way by the relation

$$\frac{dr}{dr_*} = \frac{\Delta}{r^2}. \quad (5)$$

The extremal value of the black hole charge, Q_{ext} , is given by the following function of the hole's horizon radius:

$$Q_{ext}^2 = r_+^2 \left(1 + 3r_+^2/R^2 \right). \quad (6)$$

2.2. Scalar perturbations

The scalar perturbations of the RN-AdS metric have been studied in [12], so we only give the final result. Separating the angular dependence of the perturbations and introducing a differential operator

$$\Lambda^2 = \frac{d^2}{dr_*^2} + \omega^2, \quad (7)$$

the radial part of the perturbations obeys a wave equation

$$\Lambda^2 Z = VZ \quad (8)$$

with potential

$$\begin{aligned} V &= f(r) \left[\frac{l(l+1)}{r^2} + \frac{f'(r)}{r} \right] \\ &= \frac{\Delta}{r^2} \left[\frac{l(l+1)}{r^2} + \frac{1}{r} \left(\frac{r_+}{r^2} + \frac{r_+^3}{R^2 r^2} + \frac{Q^2}{r_+ r^2} - \frac{2Q^2}{r^3} + \frac{2r}{R^2} \right) \right]. \end{aligned} \quad (9)$$

Here l is the usual spherical harmonic index. In the limit $Q = 0$ this potential reduces to the four-dimensional limit of the scalar potential considered by Horowitz and Hubeny [9].

2.3. Electromagnetic and gravitational perturbations

The electromagnetic and gravitational perturbation equations for Reissner-Norström-de Sitter black holes were considered in [5] following the track outlined in [20]. Once again, their derivation is carried over with no difficulty to the RN-AdS spacetime, so we only give the final expressions for the perturbation equations. After separation of the angular dependence, the axial perturbations (which we will denote by a superscript “-”) are described by a couple of wave equations:

$$\Lambda^2 Z_i^- = V_i^- Z_i^-. \quad (10)$$

Defining

$$n = \frac{(l-1)(l+2)}{2} \quad (11)$$

and

$$\begin{aligned} p_1 &= 3M + (9M^2 + 8nQ^2)^{1/2}, \\ p_2 &= 3M - (9M^2 + 8nQ^2)^{1/2}, \end{aligned} \quad (12)$$

the relevant potentials are

$$V_i^- = \frac{\Delta}{r^5} \left[2(n+1)r - p_j \left(1 + \frac{p_i}{2nr} \right) \right] \quad (i, j = 1, 2; i \neq j). \quad (13)$$

Similarly, the radial parts of the polar perturbations (that we will denote by a superscript “+”) obey the couple of equations:

$$\Lambda^2 Z_i^+ = V_i^+ Z_i^+, \quad (14)$$

where

$$\begin{aligned} V_1^+ &= \frac{\Delta}{r^5} \left[U + \frac{1}{2}(p_1 - p_2)W \right], \\ V_2^+ &= \frac{\Delta}{r^5} \left[U - \frac{1}{2}(p_1 - p_2)W \right]. \end{aligned} \quad (15)$$

Here U and W are given by

$$\begin{aligned} W &= \frac{\Delta}{r\varpi^2} (2nr + 3M) + \frac{1}{\varpi} \left(nr + M - \frac{2r^3}{R^2} \right), \\ U &= (2nr + 3M)W + \left(\varpi - nr - M + \frac{2r^3}{R^2} \right) - \frac{2n\Delta}{\varpi}, \end{aligned} \quad (16)$$

and the function ϖ is defined by the relation

$$\varpi = nr + 3M - \frac{2Q^2}{r}. \quad (17)$$

In the limit $Q = 0$, the potentials V_1^- and V_1^+ reduce to the corresponding potential for pure electromagnetic perturbations of Schwarzschild-AdS black holes, equation (5) in [10]:

$$V_{EM} = \Delta \frac{l(l+1)}{r^4}. \quad (18)$$

Furthermore, in the same limit, the potential V_2^- reduces to the potential for pure axial gravitational perturbations of Schwarzschild, equation (13) in [10]:

$$V_{odd} = \frac{\Delta}{r^2} \left[\frac{l(l+1)}{r^2} - \frac{6M}{r^3} \right], \quad (19)$$

and the V_2^+ potential reduces to the potential describing pure polar gravitational perturbations of Schwarzschild, equation (17) in [10]:

$$V_{even} = \left(\frac{2\Delta}{r^5} \right) \frac{9M^3 + 3n^2Mr^2 + n^2(1+n)r^3 + 3M^2(3nr + 3r^3/R^2)}{(3M + nr)^2}. \quad (20)$$

2.4. Numerical method

In AdS backgrounds, QNM's are defined as solutions to the relevant wave equations characterized by purely ingoing waves at the event horizon and vanishing perturbation at radial infinity. We used two different numerical methods to solve this eigenvalue problem. The first has been discussed at length in previous papers [9, 10, 12], and we briefly recall it using our notation (and covering the slightly more general case considered here) in Appendix 1. As a further check, we also extended to the axial perturbations of RN-AdS black holes the Fröbenius method used in [11] for S-AdS black holes, developing on previous work for black holes in asymptotically flat spacetime [18, 19]. This extension (which essentially involves the use of a four-term recurrence relation instead of a three-term recurrence relation) is presented in Appendix 2.

The two methods yield numerical results which agree to machine accuracy. In both formulations of the eigenvalue problem, we numerically search for roots in the plane (ω_R, ω_I) using Müller's method. For pure-imaginary roots, it is sometimes convenient to resort to Ridder's method (for a description of both root-searching techniques, see e.g. [21]). The Fröbenius method is computationally much faster, and it is also easier to implement. However, at variance with the asymptotically flat case, axial and polar perturbations in anti-de Sitter backgrounds are not isospectral [10]. A similar isospectrality breaking was found for perturbations of charged, dilaton black holes in [22]. As a consequence, polar perturbations, which are described by the rather messy potentials (15), cannot simply be related to axial perturbations through a Chandrasekhar transformation of the radial perturbation variables [20]. So we only used the Fröbenius method as a check when computing modes associated to the axial potentials (13).

From now on, in presenting the numerical results, we will set the AdS radius $R = 1$. It is also useful to normalize the charge to its extremal value, defining

$$\bar{Q} = Q/Q_{ext}. \quad (21)$$

Finally, we set $\omega = \omega_R - i\omega_I$, in order to have positive values for the imaginary parts of QNM frequencies. In the next sections we will first recall the properties of S-AdS QNM's, verifying and extending results found in [9, 10]. Then we will present our results for charged black holes, discussing both the scalar modes studied in [12] and the electromagnetic and gravitational perturbations, which, to our knowledge, are studied here for the first time. In both cases we will first discuss the "ordinary" QNM's, and then the purely damped QNM's (whose real part $\omega_R = 0$), which show rather peculiar features deserving special attention.

3. NUMERICAL RESULTS

3.1. Schwarzschild-anti-de Sitter black holes

3.1.1. "Ordinary" quasi-normal modes

Consider a sequence of *uncharged* black holes in anti-de Sitter space, and fix units such that the AdS radius $R = 1$. Then QNM frequencies only depend on the holes' horizon radius r_+ , and can be plotted as curves in the complex (ω_R, ω_I) plane. Such curves are shown for the fundamental scalar mode with $l = 0$ (continuous line), for the first non-purely damped axial mode with $l = 2$ (dashed line) and for the fundamental polar mode with $l = 2$ (dotted line) in figure 1. Comparing the dashed and dotted lines in the figure, it is apparent that, as mentioned in the previous paragraph, in a S-AdS background the isospectrality between even and odd perturbations (which is a property of asymptotically flat black hole spacetime perturbations) is broken. However, it is approximately restored in the large ω and in the small black hole limit (for a discussion of this property, see section III C in [10]). Scalar perturbations are isospectral with odd and even parity gravitational perturbations in the large black hole (large ω) limit. As yet, there is no analytical proof of this rather surprising feature, which we have numerically verified both for the fundamental mode and for the overtones.

In general, our results are in perfect numerical agreement with those presented in [9, 10]. In their treatment of *scalar* perturbations, Horowitz and Hubeny found that, for large black holes and $l = 0$, the real and imaginary part of QNM frequencies scale linearly with the temperature. In four dimensions, they predicted that the fundamental mode frequencies are well fitted by the relations $\omega_R = 7.75T$, $\omega_I = 11.16T$. They also found that, in general, the overtones are equally spaced, obeying relations of the form $\omega_R(n) \sim 54 + 131n$, $\omega_I(n) \sim 41 + 225n$, where n is a positive integer, not to be confused with the coefficient n defined in equation (11). As l increases, ω_I decreases and ω_R increases, but the l -dependence of the modes is extremely weak.

Our numerical results confirm all of these statements, and show that they apply also to axial and polar gravitational perturbations. Table I shows the fit parameters for the linear temperature-dependence of the lowest QNM frequencies

TABLE I: Linear scaling of the real and imaginary part of QNM frequencies with the black hole temperature for large S-AdS black holes. All fits have been obtained on a set of numerical data with black hole radii varying between $r_+ = 10$ and $r_+ = 100$ (see text). In parentheses, we show the difference between a given fitting coefficient and the fitting coefficient of the preceding mode: as the mode order grows, modes tend to become more and more equally spaced. The axial modes have been labelled starting from one to take into account the existence of a purely damped mode.

Scalar ($l = 0$)			Axial ($l = 2$)			Polar ($l = 2$)		
Mode	ω_R/T	ω_I/T	Mode	ω_R/T	ω_I/T	Mode	ω_R/T	ω_I/T
0	7.747	11.157	1	7.748	11.157	0	7.750	11.153
1	13.243	20.592	2	13.243	20.592	1	13.246	20.585
	(5.495)	(9.435)		(5.495)	(9.435)		(5.496)	(9.432)
2	18.702	30.021	3	18.702	30.021	2	18.705	30.010
	(5.458)	(9.429)		(5.459)	(9.429)		(5.459)	(9.425)
3	24.151	39.447	4	24.152	39.447	3	24.154	39.434
	(5.450)	(9.426)		(5.450)	(9.426)		(5.449)	(9.424)

with $l = 0$ (scalar case) and $l = 2$ (gravitational case). Notice that the labelling of axial QNM frequencies starts at $n = 1$, since we regard the pure imaginary mode found in [10] as the fundamental. All fits have been done on a table obtained performing explicit calculations for black holes with horizon radii varying from $r_+ = 10$ to $r_+ = 100$ in steps of $\Delta r_+ = 0.1$. Values in parentheses indicate the spacing in the fitting coefficient between a given mode and the previous overtone: as the overtone number increase, these numbers tend to a constant. It may also be noted that fitting coefficients in this large black hole limit are essentially the same for all three kinds of perturbations.

In brief, from Table I we can deduce a very simple “generalized formula”: for the fundamental mode and the overtones of *scalar and gravitational* S-AdS perturbations, QNM frequencies are well approximated by the fitting formula

$$\omega_R \sim (7.75 + 5.46n)T, \quad \omega_I \sim (11.16 + 9.43n)T. \quad (22)$$

A relabelling of the integer n is necessary to take into account the existence of a purely imaginary axial gravitational mode, but this is just a matter of convention.

3.1.2. Purely damped modes

The study of electromagnetic and gravitational quasi-normal modes for S-AdS black holes has unexpectedly revealed the existence of axial gravitational modes with pure-imaginary frequency [10]. These modes have the interesting property that their frequency does not scale linearly with the black hole radius, but rather with the *inverse* of the black hole radius: an explicit fit (performed using data in the range $r_+ = 10$ to $r_+ = 100$ at steps $\Delta r_+ = 0.1$) shows indeed that for purely damped axial modes with $l = 2$ (see Table III in [10]) $\omega_I = 1.335/r_+$.

In other words, in this case ω_I scales with the inverse of the mass, as it does for Schwarzschild black holes in flat spacetime: hence these modes are *particularly long lived*. Cardoso and Lemos managed to prove stability for other kinds of perturbations, but not for these modes. Indeed, the proof relies on the radial potential being positive, while V_{odd} , given by formula (19), can be negative for some values of l and M .

Electromagnetic perturbations of large S-AdS black holes are also characterized by a set of pure imaginary modes, which however scale in the “ordinary” way ($\omega_I \sim r_+$).

We point out that we get essentially perfect agreement with all the numerical results shown in [10], with the exception of their Table II (lowest QNM of electromagnetic perturbations for $l = 2$). The values we obtain in this particular case are given in Table II. More importantly, we find no evidence for the axial “algebraically special” mode with $r_+ = 1$ and pure-imaginary frequency $\omega_I = 2$, indicated as a “dubious” result in Table III of [10]. In both formulations of the eigenvalue problem, our two-dimensional Müller root-searching routines fail to converge there, and even a one-dimensional search on the axis $\omega_R = 0$ does not show any root. This is not too surprising. This algebraically special mode (if it exists) would be characterized by boundary conditions different from those of ordinary QNM’s: there would be no radiation going down the black hole horizon [10].

It is well known from the asymptotically flat case [20] that, as we “turn on” the charge, electromagnetic and gravitational modes become “mixed”: as we noted earlier on, only when $Q \rightarrow 0$ the potentials V_2^\pm reduce to pure gravitational perturbations of Schwarzschild, and the V_1^\pm potentials reduce to pure electromagnetic perturbations.

TABLE II: Lowest QNM of S-AdS, pure electromagnetic perturbations for $l = 2$. In parentheses we give the values listed in Table II of the paper by Cardoso and Lemos.

r_+	$\omega_R (\omega_R^{CL})$	$\omega_I (\omega_I^{CL})$
0.8	3.224 (2.501)	0.996 (1.176)
1	3.223 (2.496)	1.384 (1.579)
5	3.090 (0.822)	9.822 (10.309)
10	0	16.623 (15.755)
50	0	75.269 (75.139)
100	0	150.133 (150.069)

TABLE III: Location of minima and maxima of $\omega_R(\bar{Q})$ for the fundamental mode. Values listed correspond to some selected values of the horizon radius r_+ and to different classes of perturbations. A dash (“-”) means that our numerical method fails to converge before reaching the corresponding minimum or maximum in \bar{Q} .

r_+	Scalar ($l = 0$)		Axial ($l = 2$)		Polar ($l = 2$)	
r_+	min	max	min	max	min	max
100	0.366	0.474	0.366	0.474	0.366	0.474
50	0.366	0.474	0.366	0.474	0.366	0.474
10	0.367	0.475	0.368	0.476	0.369	0.477
5	0.372	0.480	0.376	0.483	0.376	0.488
1	0.468	0.571	-	-	0.503	-

We will see in the next section that both modes (i.e., those which can be classified as “purely electromagnetic” and “pure gravitational” in the S-AdS, $Q = 0$ limit) show an interesting behaviour as the charge increases. In particular, *purely damped* modes of both classes behave in a very peculiar way: their damping seems to go to infinity ($\omega_I \rightarrow 0$) in the extremal black hole case, suggesting the possibility that *extremally charged RN-AdS black holes may be marginally unstable to electromagnetic and gravitational perturbations*.

3.2. Reissner-Nordström-anti-de Sitter black holes

3.2.1. “Ordinary” quasi-normal modes

A first study of scalar perturbations of RN-AdS black holes was carried out by Wang, Lin and Abdalla [12]. The authors found that “switching on the charge” results in a breakdown of the linear relations $\omega_R(T)$, $\omega_I(T)$ (and in a similar breakdown of the linear relation between T and r_+) which is larger the larger is the charge. In a following paper, time evolutions of the scalar field wave equation were used to cross-check these results [15] and to study the late-time behaviour of the perturbing field. Both numerical methods used in our work (see the Appendix) are frequency-domain methods, and break down for large values of the charge, for reasons related to the radius of convergence of power-series solutions of the wave equation [12]. However, time evolutions do not suffer of this problem, and were used to show that the imaginary part of the frequency attains a maximum at some critical value of the charge Q_{crit} , to reduce again as $Q \rightarrow Q_{ext}$. This is an important point on which we will comment later.

Our numerical results for the scalar case agree with those presented in [12, 15] (for example, we are in excellent agreement with Table II in [15]), and confirm a breakdown of the linear relations (22) as the black hole charge increases. However, in [12] it was not only claimed that ω_I increases with Q , but also that ω_R decreases with Q , so that, in their words, “*if we perturb a RN-AdS black hole with high charge, the surrounding geometry will not “ring” as much and long as that of the black hole with small Q* ”. Our results do not confirm this statement.

This can be seen, for example, from figure 1. The continuous wiggling “tails” departing from the scalar-mode line are numerical solutions of the scalar eigenvalue problem for selected horizon radii and increasing charge. From the plot it is clear that, as the charge increases, the imaginary part of the frequency increases, according to the predictions in [12]; however, the real part of the frequency does not show a monotonically decreasing behaviour!

The situation is clarified in figure 2, where we also consider polar and axial perturbations. Consider first the top two panels in figure 2, where we plot the QNM frequency ω_R as a function of the normalized charge $\bar{Q} = Q/Q_{ext}$. Each

TABLE IV: Fit parameters for the charge dependence of the real part of the QNM frequency for some selected horizon radii and different classes of perturbations – see formula (23). The accuracy of these fits, which are only valid for $\bar{Q} < 1/3$, is typically of some parts in a thousand.

r_+	Scalar ($l = 0$)		Axial ($l = 2$)		Polar ($l = 2$)	
r_+	a	b	a	b	a	b
100	1.6944	3.6144	1.6943	3.6135	1.6940	3.6107
50	1.6939	3.6109	1.6935	3.6074	1.6923	3.5963
10	1.6775	3.5021	1.6771	3.4198	1.6378	3.1729
5	1.6284	3.1911	1.5882	2.9204	1.4695	2.2189

TABLE V: Fit parameters for the charge dependence of the imaginary part of the QNM frequency for some selected horizon radii and different classes of perturbations – see formula (24). The accuracy of these fits, which are only valid for $\bar{Q} < 1/3$, is typically of some parts in a hundred.

r_+	Scalar ($l = 0$)		Axial ($l = 2$)		Polar ($l = 2$)	
r_+	c	d	c	d	c	d
100	0.56827	5.8567	0.56829	5.8556	0.56892	5.8550
50	0.56839	5.8524	0.56847	5.8483	0.57096	5.8458
10	0.57193	5.7182	0.57378	5.6222	0.63597	5.5560
5	0.58145	5.3361	0.58634	5.0124	0.83131	4.7163

panel corresponds to a different value of r_+ . As we could expect from the uncharged black hole limit, the scalar and mixed gravitational/electromagnetic perturbations are *almost isospectral for large black holes*, but the isospectrality breaks down for intermediate-size holes. Quite interestingly, QNM frequencies show indeed some kind of “damped oscillations” as Q increases. In Table III we list the location of minima and maxima in $\omega_R(\bar{Q})$ for the three different kinds of perturbations, and for selected values of r_+ . For large black holes (which are of greater interest in view of the AdS/CFT correspondence), the values of \bar{Q} for which the frequency attains the local minimum and maximum are *independent of the black hole radius*: they correspond, respectively, to $\bar{Q} = 0.366$ and $\bar{Q} = 0.474$.

For small values of the charge, $\bar{Q} < 1/3$, an excellent fit of the real part of the frequency at fixed r_+ (errors are typically of order 10^{-4} or smaller, especially for the low-order modes), valid for all kinds of perturbations, is provided by a simple polynomial relation:

$$\omega_R = \omega_R^{(0)} (1 - a\bar{Q}^2 - b\bar{Q}^4), \quad (23)$$

where we have denoted by $\omega_R^{(0)}$ the real part of the QNM frequency in the zero-charge (S-AdS) limit. The fit parameters a and b are given for selected values of r_+ in Table IV. Again, they are largely independent of r_+ and of the kind of perturbation considered, at least in the large black hole limit.

Let us now turn to the bottom two panels in figure 2. For the values of the charge allowed by our numerical methods, ω_I increases monotonically as \bar{Q} increases. The second derivative of $\omega_I(\bar{Q})$ changes sign when the real part of the frequency attains the local minimum, and then again at the local maximum. A good fit in the region $\bar{Q} < 1/3$ (errors being of the order of a few percent for the fundamental mode, and of order 1 % or less for the overtones) is again obtained using a polynomial relation:

$$\omega_I = \omega_I^{(0)} (1 + c\bar{Q}^2 + d\bar{Q}^4), \quad (24)$$

where we denote by $\omega_I^{(0)}$ the imaginary part of the QNM frequency in the S-AdS limit. The fit parameters c and d are listed in Table V. As for the fitting coefficients of the real part, c and d are largely independent of r_+ and of the kind of perturbation considered in the large black hole limit.

Summarizing, for large black holes with charge $\bar{Q} < 1/3$, QNM frequencies and dampings are approximated within about 1 % by a very simple formula:

$$\begin{aligned} \omega_R &= (7.75 + 5.46n)T^{(0)} (1 - 1.694\bar{Q}^2 - 3.61\bar{Q}^4), \\ \omega_I &= (11.16 + 9.43n)T^{(0)} (1 + 0.568\bar{Q}^2 + 5.86\bar{Q}^4), \end{aligned} \quad (25)$$

where $T^{(0)} = (1 + 3r_+^2)/4\pi r_+$ is the S-AdS (uncharged) black hole temperature. Notice that, for fixed Q , the dependence of ω_R and ω_I on the angular index l is extremely weak, so this formula holds with good accuracy also for angular multipoles larger than the fundamental.

3.2.2. Purely damped modes: are extreme RN-AdS black holes marginally unstable?

Modes which become “purely electromagnetic” or purely imaginary in the S-AdS limit deserve a separate discussion.

Let us first consider the pure-imaginary modes for axial gravitational perturbations. In figure 3 we “track” the imaginary part of these modes, starting from the corresponding zero-charge limit, for different values of the horizon radius. As explained when we discussed purely imaginary QNM’s for S-AdS black holes, our numerical results do not confirm the existence of an algebraically special mode in the zero-charge limit at $r_+ = 1$: as we decrease r_+ , the root finder breaks down when $r_+ \sim 1.04$ (dashed line in the plot), corresponding to a S-AdS frequency $\omega_I = 1.860$.

It is clear from the plot that all modes show a tendency to approach the horizontal axis as the charge approaches the extremal value. This tendency is much clearer if we use a linear scale (instead of the log scale used in this plot, which is necessary to display all modes together). Unfortunately, for the convergence reasons discussed earlier, we cannot push our calculations to the extremal limit. However, our plots lead us to conjecture that *all pure-imaginary axial modes are such that $\omega_I \rightarrow 0$ as $Q \rightarrow Q_{ext}$.*

Our conjecture finds firmer ground in the behaviour of the modes for the V_1^- potential which reduce to purely-damped electromagnetic perturbations with $l = 1$ and $l = 2$ in the S-AdS limit. In this case, we were able to track roots for all values of the charge $\bar{Q} < 1$, and our results are shown in the two panels of figure 4: the imaginary part of purely-electromagnetic modes in the Schwarzschild limit *does* indeed tend to zero as $\bar{Q} \rightarrow 1$.

For small black holes, such a behaviour is not observed. Small black holes in S-AdS do not have pure imaginary electromagnetic modes. Tracking again the modes of the V_1^- potential (figure 5) we see that their real part decreases as a function of Q , but the imaginary part does not: indeed, $\omega_I(Q)$ is decreasing when $r_+ \gtrsim 2$, but it shows a relative minimum when $r_+ = 1.5$, and is roughly constant or slowly increasing when $r_+ \lesssim 1$!

Our results suggest the possibility that, *unless the mode amplitude tends to zero in the extremal limit, large extremal RN-AdS black holes are marginally unstable to electromagnetic (and perhaps, axial gravitational) perturbations.* This result may be extremely interesting in view of the AdS/CFT conjecture.

We only make a couple of comments at this stage. First, notice that even for S-AdS black holes, a proof of stability to large black hole, axial gravitational perturbations does not exist [10]. Second, as we recalled earlier, time evolutions of scalar fields in RN-AdS spacetimes have shown that, for Q greater than some critical value Q_{crit} , ω_I is a *decreasing* function of charge [15]. The authors suggested a possible connection between this behaviour and the existence of a second-order phase transition for extremal RN-AdS black holes [23]. Development of more efficient numerical methods is needed to verify such a connection between QNM’s and thermodynamical phase transitions of extremal RN-AdS black holes. An understanding of the link between our study and the dynamical instability discussed by Gubser and Mitra [24, 25], which in their words persists “*for finite size black holes in AdS, down to horizon radii on the order of the AdS radius*”, could shed further light on the AdS/CFT conjecture. We notice that an interesting discussion of the connection between dynamical and thermodynamical stability in AdS spacetimes can be found in [26].

4. CONCLUSIONS

We have studied scalar, electromagnetic and gravitational perturbations of a RN-AdS spacetime, and computed its QNM’s. Our results extend previous computations carried out for scalar, electromagnetic and gravitational perturbations of S-AdS black holes [9, 10] and for scalar perturbations of RN-AdS black holes [12]. For “large” black holes, whose horizon is much larger than the AdS radius, different kinds of perturbations are almost exactly *isospectral*; this isospectrality is broken when the black hole’s horizon radius is comparable to the AdS radius. Contrary to previous claims, we find that, as the black hole charge Q increases, the real part of the QNM frequency does not continuously decrease, but rather shows a minimum followed by a maximum. The location of these extrema as a function of $\bar{Q} = Q/Q_{ext}$ is independent of the black hole radius for large black holes: minima are located at $\bar{Q} = 0.366$, and maxima at $\bar{Q} = 0.474$. We found that the imaginary part of the QNM frequency ω_I is generally, at least for small values of Q , an increasing function of the black hole charge, whose second derivative changes sign corresponding to the minima and maxima of $\omega_R(\bar{Q})$. We also obtained the very accurate fitting formulas (25), which are valid for large black holes having charge $Q < Q_{ext}/3$.

A very interesting result concerns electromagnetic and axial perturbations of large black holes. These perturbations are characterized by the existence of purely damped modes. We advanced numerical evidence that the damping of these modes approaches infinity as the black hole charge approaches the extremal value. If the corresponding mode

amplitude does not tend to zero, this would imply that *extremally charged RN-AdS black holes are marginally unstable*. Our results are relevant in view of the AdS/CFT conjecture, since, according to it, the AdS QNM's yield thermalization timescales in the corresponding conformal field theory. It would be desirable to relate our results to the existence of a second-order phase transition for extremal RN-AdS black holes [23] and to a dynamical instability which has been studied in the past [24, 25], and which also holds for finite size RN-AdS black holes having horizon radii larger than the AdS radius. We believe that investigating these connections could clarify many issues related to the AdS/CFT correspondence.

Acknowledgments

This work has been supported by the EU Programme 'Improving the Human Research Potential and the Socio-Economic Knowledge Base' (Research Training Network Contract HPRN-CT-2000-00137).

APPENDIX A: NUMERICAL COMPUTATION OF QUASINORMAL MODES

1. The Horowitz–Hubeny method

Here we briefly describe the first numerical method we used to compute the quasinormal modes. This method has been described elsewhere [9, 10, 12], so we only give the essential formulas, which encompass the slightly more general case considered here. For a generic wavefunction obeying one of the five wave equations (8), (10) or (15), write

$$\psi(r) = e^{i\omega r_*} Z(r) \quad (\text{A1})$$

and get the equation for $\psi(r)$

$$f(r) \frac{\partial^2 \psi(r)}{\partial r^2} + [f'(r) - 2i\omega] \frac{\partial \psi(r)}{\partial r} - \tilde{V}(r) \psi(r) = 0, \quad (\text{A2})$$

where $\tilde{V}(r) = V(r)/f(r)$. Introducing a new variable $x = 1/r$ to “compactify” the region outside the black hole, and defining $x_+ = 1/r_+$, this equation is rewritten as

$$s(x) \frac{d^2 \psi(x)}{dx^2} + \frac{t(x)}{x - x_+} \frac{d\psi(x)}{dx} + \frac{u(x)}{(x - x_+)^2} \psi(x) = 0 \quad (\text{A3})$$

where

$$s(x) = \frac{r_0 x^5 - x^4 - x^2 - Q^2 x^6}{x - x_+}, \quad (\text{A4})$$

$$t(x) = 3r_0 x^4 - 2x^3 - 4Q^2 x^5 - 2i\omega x^2, \quad (\text{A5})$$

$$u(x) = (x - x_+) \tilde{V}(x), \quad (\text{A6})$$

and

$$r_0 = \frac{1 + x_+^2 + Q^2 x_+^4}{x_+^3}. \quad (\text{A7})$$

Now look for a series solution in the form

$$\psi(x) = \sum_{k=0}^{\infty} a_k (x - x_+)^k. \quad (\text{A8})$$

This series solution obeys the boundary conditions required for quasinormal modes if the condition

$$\psi(0) = \sum_{k=0}^{\infty} a_k (-x_+)^k = 0 \quad (\text{A9})$$

is satisfied. The coefficients $a_k = a_k(\omega)$ can be obtained through the following recursion relation:

$$a_j = -\frac{1}{P_j} \sum_{k=0}^{j-1} [k(k-1)s_{j-k} + kt_{j-k} + u_{j-k}] a_k. \quad (\text{A10})$$

In this formula the s_k 's, t_k 's and u_k 's are coefficients in a Taylor series expansion around $x = x_+$ of the functions $s(x)$, $t(x)$ and $u(x)$ respectively, and

$$P_j = j(j-1)s_0 + jt_0. \quad (\text{A11})$$

2. The Fröbenius method

As a check of our results, we have applied an alternative method, originally suggested by Leaver [18] and applied in [11] to the axial perturbations of S-AdS BHs. We have generalized the approach to RN-AdS BHs. Since this method is computationally much faster, and very easy to implement for the axial potentials V_1^- and V_2^- , we give the details here.

Rewrite equation (A3) multiplying it by $(x - x_+)/x^2$ to find:

$$p(x) \frac{d^2\psi(x)}{dx^2} + q(x) \frac{d\psi(x)}{dx} + \frac{\tilde{V}(x)}{x^2} \psi(x) = 0 \quad (\text{A12})$$

where as usual $\tilde{V} = V/f$, and furthermore

$$\begin{aligned} p(x) &= (2Mx^3 - x^2 - 1 - Q^2x^4), \\ q(x) &= (6Mx^2 - 2x - 4Q^2x^3 - 2i\omega). \end{aligned} \quad (\text{A13})$$

Now look for the solution in the form of a Fröbenius series which is regular at the event horizon:

$$u(x) = \sum_{n=0}^{\infty} a_n \left(\frac{x - x_+}{-x_+} \right)^n, \quad (\text{A14})$$

where $a_0 = 1$.

In the RN-AdS case, as is the case for Reissner-Nordström black holes in asymptotically flat spacetimes [19], the expansion coefficients are determined by a four-term recurrence relation of the form:

$$\begin{aligned} \alpha_0 a_1 + \beta_0 a_0 &= 0, \\ \alpha_1 a_2 + \beta_1 a_1 + \gamma_1 a_0 &= 0, \\ \alpha_n a_{n+1} + \beta_n a_n + \gamma_n a_{n-1} + \delta_n a_{n-2} &= 0, \quad n = 2, 3, \dots \end{aligned} \quad (\text{A15})$$

where the recursion coefficients are given in terms of the parameters appearing in the black hole potentials V_i^- , defined in equation (13), as follows:

$$\begin{aligned} \alpha_n &= 2(n+1) [(n+1)(1 - 3Mx_+ + 2Q^2x_+^2) + i\omega/x_+], \\ \beta_n &= n(n+1) (6Mx_+ - 1 - 6Q^2x_+^2) + l(l+1) - p_j x_+ - \frac{p_i p_j}{2n} x_+^2, \\ \gamma_n &= (n^2 - 1) (4Q^2x_+^2 - 2Mx_+) + p_j x_+ + \frac{p_i p_j}{n} x_+^2, \\ \delta_n &= -(n-2)(n+1)Q^2x_+^2 - \frac{p_i p_j}{2n} x_+^2. \end{aligned} \quad (\text{A16})$$

In the zero-charge limit $Q = 0$ we recover a standard, three term recursion relation [11]. Once the a_n 's are known (in practice, up to some finite value of n determined by the accuracy we want to achieve), the QNM's are determined by imposing the condition $u(x=0) = 0$.

[1] K.D. Kokkotas, B.G. Schmidt, Living Rev. Relativ. **2**, 2 (1999).

- [2] H.-P. Nollert, CQG **16**, R159-R216 (1999).
 [3] J. Guven, D. Nuñez, PRD **42**, 2577 (1990).
 [4] H. Otsuki, T. Futamase, Prog. Theor. Phys. **85**, n. 4, 771 (1991).
 [5] F. Mellor, I. Moss, PRD **41**, 403 (1990).
 [6] J. Maldacena, Adv. Theor. Math. Phys. **2**, 253 (1998).
 [7] D. Birmingham, I. Sachs, S. N. Solodukhin, hep-th/0212308 (2003).
 [8] J. Chan, R. Mann, PRD **55**, 7546 (1997); **59**, 064025 (1999).
 [9] G.T. Horowitz, V.E. Hubeny, PRD **62**, 024027 (2000).
 [10] V. Cardoso, J.P.S. Lemos, PRD **64**, 084017 (2001).
 [11] I.G. Moss, J.P. Norman, gr-qc/0201016 (2002).
 [12] B. Wang, C.Y. Lin, E. Abdalla, Phys. Lett. B **481**, 79 (2000).
 [13] P.R. Brady, C.M. Chambers, W. Krivan, P. Laguna, PRD **55**, 7538 (1997).
 [14] P.R. Brady, C.M. Chambers, W.G. Laarakkers, E. Poisson, PRD **60**, 064003 (1999).
 [15] B. Wang, C. Molina, E. Abdalla, PRD **63**, 084001 (2001).
 [16] R.A. Konoplya, PRD **66**, 044009 (2002).
 [17] J.-M. Zhu, B. Wang, E. Abdalla, PRD **63**, 124004 (2001).
 [18] E. W. Leaver, Proc. Roy. Soc. Lon. **A402**, 285 (1985).
 [19] E. W. Leaver, PRD **41**, 2986 (1990).
 [20] S. Chandrasekhar, in *The Mathematical Theory of Black Holes* (Oxford University, New York, 1983).
 [21] W. H. Press, S. A. Teukolsky, W. T. Vetterling, B. P. Flannery, in *Numerical Recipes* (Cambridge University Press, Cambridge, England, 1992).
 [22] V. Ferrari, M. Pauri, F. Piazza, PRD **63**, 064009 (2001).
 [23] A. Chamblin, R. Emparan, C.V. Johnson, R.C. Myers, PRD **60**, 064018 (1999).
 [24] S.S. Gubser, I. Mitra, hep-th/9904197 (1999).
 [25] S.S. Gubser, I. Mitra, JHEP **8**, 018 (2001).
 [26] V.E. Hubeny, M. Rangamani, JHEP **0205**, 027 (2002).

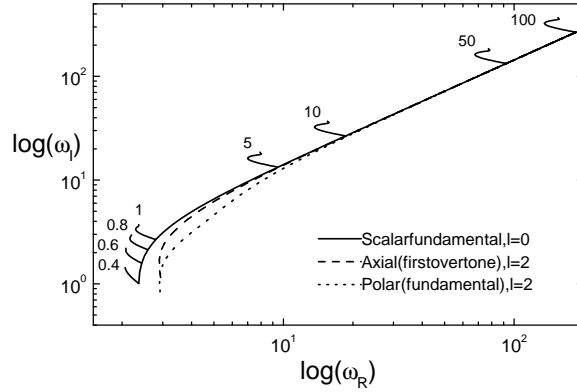


FIG. 1: Plot of the S-AdS QNM frequencies for the fundamental scalar mode with $l = 0$ (continuous line), for the first non-purely damped axial mode with $l = 2$ (dashed line) and for the fundamental polar mode for $l = 2$ (dotted line). All calculations are started at $r_+ = 100$ (top right of the diagram). The step in r_+ is reduced by $\Delta r_+ = 0.1$ and the calculation is iterated until our numerical code fails to converge (bottom left). Corresponding to selected values of the horizon radius (namely, $r_+ = 100, 50, 10, 5, 1, 0.8, 0.6, 0.4$, whose S-AdS frequencies are tabulated in Table I of Horowitz and Hubeny), we “switch on” the charge and follow the modes in the complex plane. The resulting trajectories are the “tails” departing from the continuous scalar QNM line. Axial and polar perturbations are almost isospectral both in the large and in the small black hole limit.

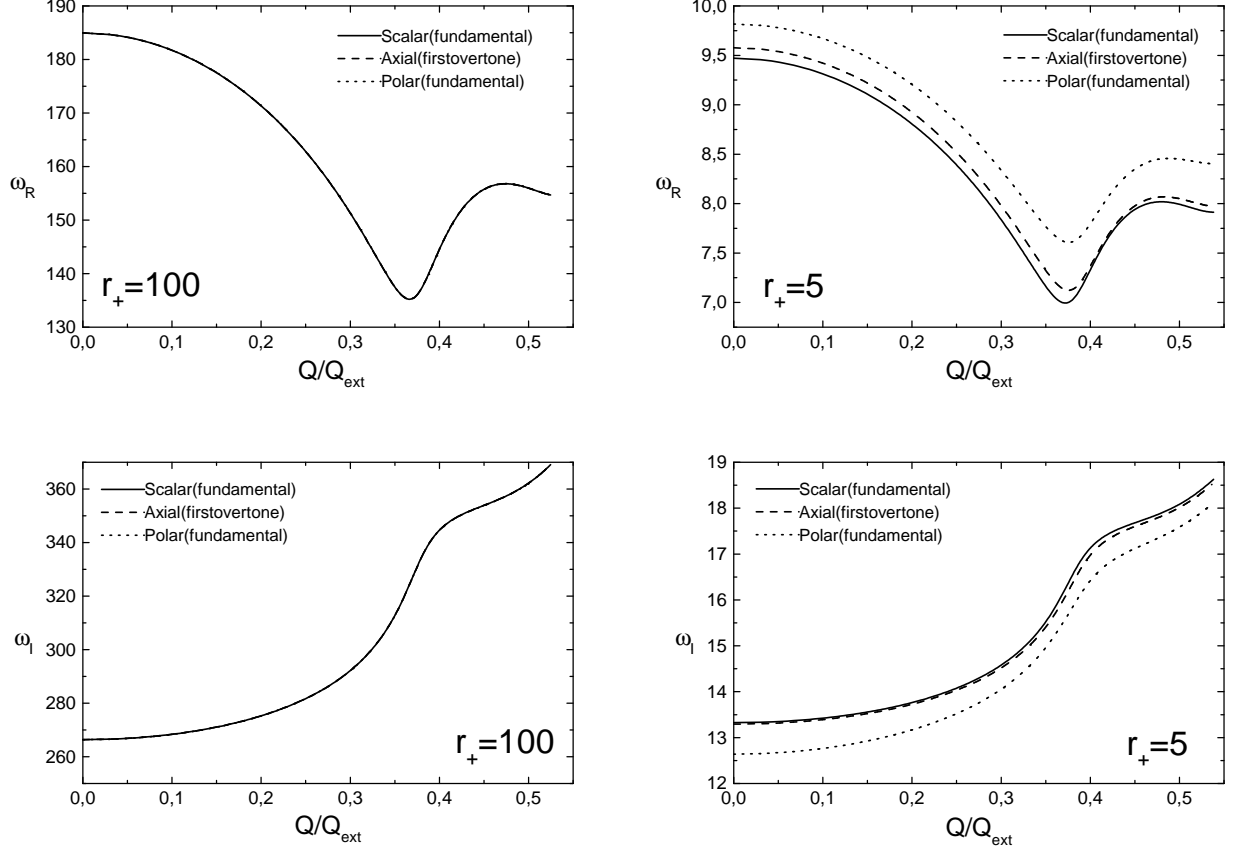


FIG. 2: The top two panel shows the characteristic “wiggling” of the real part of the QNM frequency, ω_R , as a function of the normalized charge $Q = Q/Q_{\text{ext}}$, for selected values of the horizon radius r_+ ; the bottom two panels show the imaginary part of the QNM frequency, $\omega_I(\bar{Q})$, for the same black holes. Scalar perturbations are denoted by solid lines, axial perturbations by dashed lines, and polar perturbations by dotted lines. The isospectrality of different kinds of perturbations, which holds in the large black hole limit, is clearly lost as the black hole “size” becomes comparable to the AdS radius, $r_+ \sim 1$. Notice that $\omega_I'(\bar{Q}) = 0$ when $\omega_R'(\bar{Q}) = 0$ (a prime denoting differentiation with respect to Q).

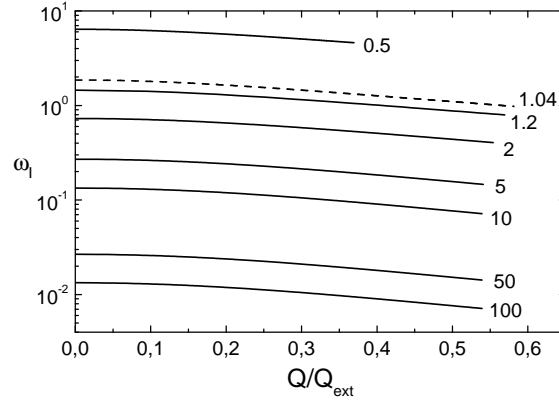


FIG. 3: Imaginary part of the purely damped mode reducing to pure axial gravitational perturbations with $l = 2$ in the zero-charge limit. Starting from S-AdS results, we track the modes for selected values of the horizon radius r_+ (indicated to the right of each curve). The calculation is terminated when our root finder fails to converge. The dashed line indicates the last mode we can find before the numerical method breaks down as we approach the “algebraically special” ($\omega_I = 2$, $r_+ = 1$) frequency.

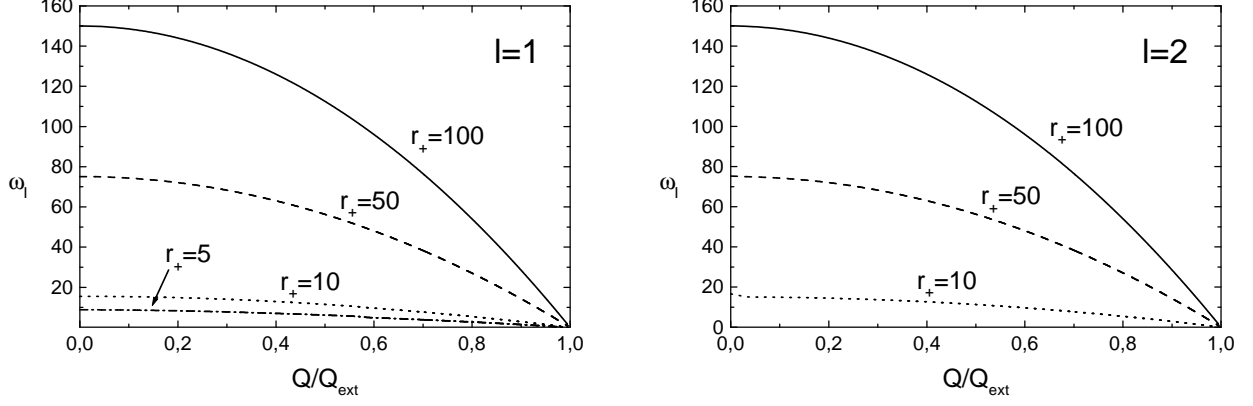


FIG. 4: Imaginary part of the purely damped mode reducing to pure electromagnetic perturbations with $l = 1$ (left panel) and $l = 2$ (right panel) in the zero-charge limit. Continuous, dashed and dotted lines refer, respectively, to black holes having horizon radius $r_+ = 100$, 50 and 10 (top to bottom in the plots). For $l = 1$, we also plot the pure imaginary mode with $r_+ = 5$ (dash-dotted line).

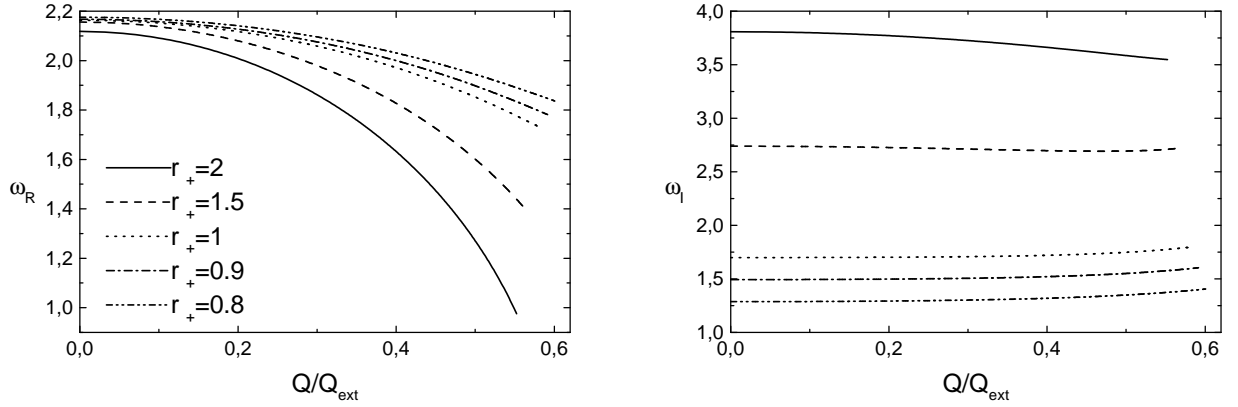


FIG. 5: Real (left panel) and imaginary parts (right panel) of the small-black hole QNM frequencies for modes reducing to pure electromagnetic perturbations with $l = 1$ in the zero-charge limit. The size of the black hole horizon radius corresponding to each curve is indicated in the inlay.